Journal of Power Sources 237 (2013) 52–57

Contents lists available at SciVerse ScienceDirect

Journal of Power Sources

journal homepage: www.elsevier.com/locate/jpowsour

Electrochemical and structural investigation of $NaCrO_2$ as a positive electrode for sodium secondary battery using inorganic ionic liquid NaFSA–KFSA

Chih-Yao Chen [a], Kazuhiko Matsumoto [a], Toshiyuki Nohira [a,*], Rika Hagiwara [a,*], Atsushi Fukunaga [a,b], Shoichiro Sakai [b], Koji Nitta [b], Shinji Inazawa [b]

[a] Graduate School of Energy Science, Kyoto University, Sakyo-ku, Kyoto 606-8501, Japan
[b] Sumitomo Electric Industries Ltd., 1-1-3 Shimaya, Konohana-ku, Osaka 554-0024, Japan

HIGHLIGHTS

- The performance of $NaCrO_2$ positive electrode was evaluated at 363 K.
- NaFSA–KFSA was used as an intermediate temperature inorganic electrolyte.
- The phase transition behavior of $NaCrO_2$ during desodiation was clarified.
- The phase transition occurred more readily at 363 K compared to room temperature.
- The reaction kinetics was enhanced at 363 K, giving the improved rate capability.

ARTICLE INFO

Article history:
Received 28 November 2012
Received in revised form
26 February 2013
Accepted 1 March 2013
Available online 14 March 2013

Keywords:
Sodium secondary battery
$NaCrO_2$
Positive electrode
Structural analysis
Ionic liquid
Bis(fluorosulfonyl)amide

ABSTRACT

The electrochemical performance of $NaCrO_2$ as a positive electrode material for an intermediate-temperature sodium secondary battery was evaluated in an inorganic ionic liquid, NaFSA–KFSA (FSA = bis(fluorosulfonyl)amide), at 363 K. The positive electrode using $NaCrO_2$, acetylene black, and polytetrafluoroethylene exhibited a stable discharge capacity of 113 mA h g^{-1} at a current density of 125 mA g^{-1}. The Coulombic efficiency and the capacity retention at the 100th cycle were 99.6% and 98.5%, respectively. Even at the very high current density of 2000 mA g^{-1}, the discharge capacity was maintained at 63 mA h g^{-1}. X-ray diffraction analyses revealed that the deintercalation of Na^+ ion from $NaCrO_2$ was associated with several phase transitions in the following sequence: rhombohedral O3, monoclinic O′3, and monoclinic P′3.

1. Introduction

Sodium secondary batteries have lately emerged as attractive energy storage systems with excellent potential for the development of affordable storage technologies, offering the prospect of lessening the dependence on Li-ion technology [1–8]. As a less expensive option, the development of Na-based batteries should accelerate the adoption of rechargeable batteries in large-scale applications such as electric grids or electric vehicles [9]. Moreover, the chemical similarity between sodium and lithium should facilitate cross-application of the huge body of knowledge regarding Li-ion technology. Most importantly, Na technology does not simply mirror the Li-ion counterpart, but presents significant unexplored opportunity and possibility [10]. Early research on sodium-based batteries has focused on high-temperature Na/S and $Na/NiCl_2$ systems that utilize the β″-Al_2O_3 solid electrolyte [11–13]. Although Na/S and $Na/NiCl_2$ batteries have been commercialized, strict thermal management is indispensable for delivering satisfactory performance [14]. The sophisticated engineering and materials necessary for ensuring durability and safety during elevated-temperature (573–623 K) operations inflate the cost and decrease the total energy density of these batteries [15]. In this respect, Na-ion battery using organic electrolytes that is operative at room temperature has been proposed [16–22]. The most common electrolyte formulations employ $NaClO_4$ or $NaPF_6$ in carbonate ester solvents, particularly propylene carbonate (PC) [3–6,16–22]. However, since these organic electrolytes are volatile and flammable, their use poses

* Corresponding authors. Tel.: +81 75 753 5822; fax: +81 75 753 5906.
E-mail addresses: nohira@energy.kyoto-u.ac.jp (T. Nohira), hagiwara@energy.kyoto-u.ac.jp (R. Hagiwara).

0378-7753/$ – see front matter © 2013 Elsevier B.V. All rights reserved.
http://dx.doi.org/10.1016/j.jpowsour.2013.03.006

safety risks and limits the battery operation temperature range [23,24].

For such reasons, the replacement of organic carbonate-based electrolytes with non-flammable and non-volatile ionic liquids appears to be a promising option [25–28]. Our prior exploration of a new class of intermediate-temperature ionic liquids consisting of alkali metal cations and either bis(trifluoromethylsulfonyl)amide (TFSA) anions or bis(fluorosulfonyl)amide (FSA) anions [29–32] demonstrated that these ionic liquids have highly desirable characteristics as battery electrolytes, such as excellent thermal stability and a wide electrochemical window. Moreover, the melting points of these salts are significantly lowered by the combination of two or three such components in prescribed compositions [29–32]. Selected eutectic mixtures have been examined as electrolytes for rechargeable batteries and the LiTFSA–KTFSA–CsTFSA and NaTFSA–CsTFSA systems have emerged as interesting candidates for lithium [33] and sodium secondary batteries [34], respectively. Test cells utilizing these ionic liquids exhibited good cycle performance and acceptable rate capability at 423 K. We recently demonstrated the feasibility of the NaFSA–KFSA ionic liquid for use in a sodium secondary battery that was operative around 363 K [35,36]. Since the salts proposed as electrolytes consist entirely of alkali metal cations and electrochemically stable amide anions, the electrochemical instability originating from organic anions and organic solvents is essentially eliminated. Detailed characterization of the NaFSA–KFSA ionic liquid including viscosity, ionic conductivity, and density has been reported in our previous paper [35].

The performance and operational safety of a battery is directly linked to the choice of electrolyte and finding suitable active materials for both positive and negative electrodes is essential for improving the overall performance of a battery. Sodium, being larger in size than lithium and also due to its greater screening effect, has a strong tendency to favor the formation of layered compounds [37]. The sodium layered oxide positive electrode materials (generally formulated as Na_xMO_2) evaluated thus far can be classified into two main groups, i.e., the O3-type and P2-type, in which the sodium ions are coordinated in octahedral and prismatic environments, respectively [3,38]. The number in this expression (e.g., 3 in O3) describes the number of transition metal (M) layers along the stacking direction in the unit cell [38]. During battery operation, the sodium ion is reversibly intercalated/deintercalated into/from these compounds; however, the cycle property and rate capability are limited relative to the Li-ion counterparts due to the larger ionic radius (1.02 Å) of Na relative to Li (0.76 Å) [37]. More in-depth research into and fundamental understanding of the structural evolution of the electrode during the entire Na intercalation/deintercalation process are needed to push the technology forward. Efforts toward this end by Delmas et al. have demonstrated the occurrence of reversible phase transitions of various Na_xCoO_2 polymorphs occurred reversibly in electrochemical sodium cells [39–41]. For example, P2–Na_xCoO_2 exhibited numerous two-phase regions in the potential curve during electrochemical desodiation. The formation of Na^+/vacancy ordered lamellar structures was confirmed via in-situ X-ray diffraction analysis [39] and it was also shown that the rhombohedral O3–$NaCoO_2$ can undergo transformation to a monoclinic distorted P′3 structure [41]. The phase transition between O3 and P3 is associated with the gliding of MO_2 slabs with respect to each other, and it is generally sensitive to the sodium content. Komaba et al. later showed that the electrochemically driven Na intercalation/deintercalation into/from $NaCrO_2$ was associated with the O3, distorted O′3 and P′3 phase transitions [21]. Similar interconvertions between O-type and P-type have also been observed in solid solutions of Na_xMO_2 such as $NaNi_{0.5}Mn_{0.5}O_2$, $NaNi_{1/3}Mn_{1/3}Co_{1/3}O_2$, and $Na_{2/3}Ni_{1/3}Mn_{2/3}O_2$ [20,37,42], although little is understood about this transformation and its effect on the kinetics of sodiation/desodiation [10].

We have previously reported the cell performance of a sodium secondary battery using the $NaCrO_2$ positive electrode in NaTFSA–CsTFSA at 423 K [34] and in NaFSA–KFSA at 353 K [35]. The present study focuses on the detailed electrochemical and structural behavior of $NaCrO_2$ in NaFSA–KFSA at 363 K with the objective of understanding the sodiation/desodiation mechanism. The obtained structural characterization and electrochemical properties are compared with previous reports in which a conventional organic electrolyte was employed at room temperature.

2. Experimental

Analytical-grade chemical reagents were used throughout and air-sensitive materials were treated under a dry Ar atmosphere. The $NaCrO_2$ powder was synthesized by means of the conventional solid-state reaction of stoichiometric Na_2CO_3 (Wako Pure Chemicals, purity >99.9%) and Cr_2O_3 (Wako Pure Chemicals, purity >98%) at 1123 K for 5 h under argon flow [35]. NaFSA and KFSA (Mitsubishi Materials Electronic Chemicals, purity 99.0%) were purchased and dried under vacuum at 333 K for 24 h.

The positive electrode was fabricated by mixing $NaCrO_2$ with acetylene black (Wako Pure Chemicals, purity >99.99%) and polytetrafluoroethylene (PTFE; Sigma–Aldrich) at a weight ratio of 85:10:5. The active material load was about 2.5 mg cm^{-2}. Metallic sodium discs (Sigma–Aldrich, purity >99.85%) were pressed on nickel current collectors and used as reference and counter electrodes. A eutectic mixture of NaFSA and KFSA (56:44, w/w) was used as the electrolyte and a glass microfiber filter (Whatman GF/A) was used as a separator. The separator was impregnated with the electrolyte under vacuum prior to the test.

Galvanostatic charge/discharge cycles were performed with a half-cell in the voltage range between 2.5 and 3.5 V. Cyclic voltammetry (CV) experiments were also carried out at various different scan rates (0.1, 0.2, and 0.5 mV s^{-1}). All electrochemical measurements were conducted at 363 K using an electrochemical workstation (VSP, Bio-Logic). All of the specific capacities in the following sections are calculated based on the mass of active material.

For the ex-situ XRD study, the Na_xCrO_2 samples were prepared in the sodium cells by applying a constant oxidation current (10 mA g^{-1}) to $NaCrO_2$ for a given duration to fix the amount of extracted sodium. Subsequently, the electrodes removed from the cells were rinsed with anhydrous tetrahydrofuran (THF; Wako Pure Chemicals, water content < 10 ppm) to remove the electrolyte and placed in an air-tight sample holder inside a glove box. Powder X-ray diffraction (XRD) patterns were recorded on a Rigaku Ultima IV instrument under a He atmosphere using Cu-Kα radiation at room temperature. The measurements were performed at 40 kV and 40 mA in the 2θ range of 10°–80° with a step size of 0.02°.

3. Results and discussion

$NaCrO_2$ was obtained as fine-grain powder with a gray–green color. All the peaks in the XRD pattern shown in Fig. 1(a) can be indexed to rhombohedral O3-type $NaCrO_2$ (*R-3m* space group, JCPDS card No. 25-0819). A typical scanning electron microscope (SEM) image of the $NaCrO_2$ powder is shown in Fig. 1(b). The individual particles consist of primary particles of $NaCrO_2$ and have diameters of about 10 μm.

The electrochemical performance of $NaCrO_2$ was evaluated using a half-cell. The CV curves for the $NaCrO_2$ electrode recorded at scan rates of 0.1, 0.2, and 0.5 mV s^{-1} are shown in Fig. 2. The $NaCrO_2$ electrode underwent Na intercalation/deintercalation with several

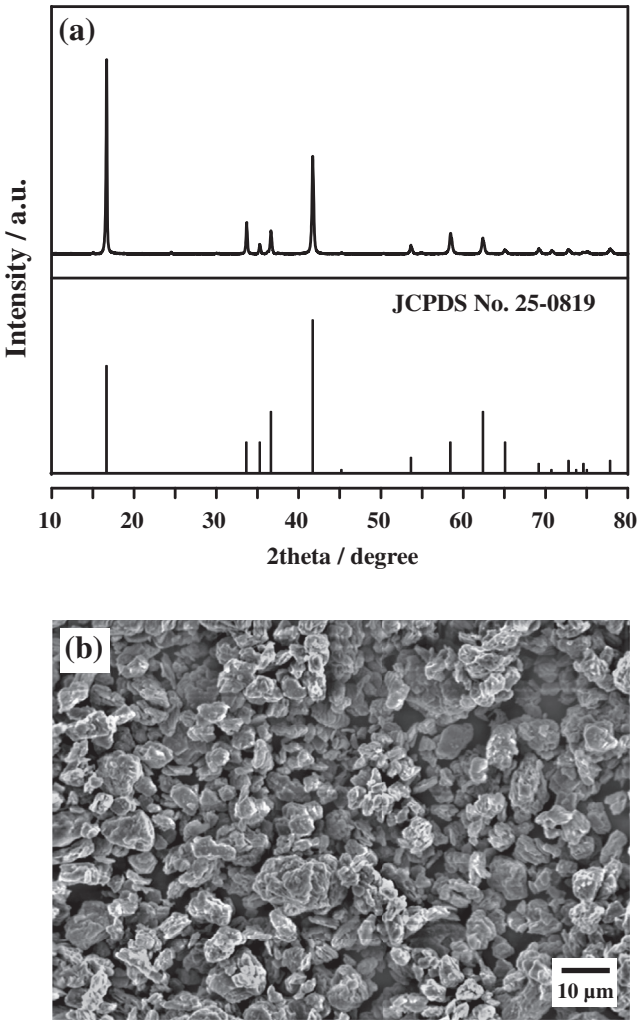

Fig. 1. (a) Powder X-ray diffraction pattern and (b) SEM image of $NaCrO_2$ powder.

reversible phase transitions evidenced as pairs of redox peaks that are clearly observed in each CV profile. The clear peak separation in each of the CV profiles indicates that the Na intercalation/deintercalation processes into/from $NaCrO_2$ are associated with the formation of distinct phases [43,44]. The shapes and areas of the redox waves remain largely unchanged during the successive scans at the various rates, indicating that reversible redox reactions occur within this potential range. It should be noted that the redox peak resolution in the present work is better than previous results obtained at room temperature [45], reflecting the faster electrode kinetics at the intermediate temperature of 363 K. The potential difference (ΔE_p) between the anodic peak and the corresponding cathodic peak gradually increases with increasing scan rate, comparable to previous reports for lamellar Na_xMO_2 materials [44].

The discharge capacity and the rate capability of the $NaCrO_2$ electrode were examined as shown in Fig. 3. A large specific capacity of 113 mA h g^{-1} was observed at a current density of 125 mA g^{-1}. Even at the very high current density of 2000 mA g^{-1}, a reversible capacity of 63 mA h g^{-1} was retained. This rate capability is comparable to the layered positive electrode for lithium ion batteries [46], which is attributed to faster kinetics at the elevated temperature (363 K). The result confirms that a moderately elevated operating temperature effectively enhances the kinetics of the Na intercalation/deintercalation processes.

The $NaCrO_2$ electrode also exhibits stable cycling properties as shown in Fig. 4. Approximately 98% of the initial capacity is maintained at the 100th cycle with a Coulombic efficiency of 99.6% at a cycling current of 125 mA g^{-1}. The average capacity fading is less than 0.02% per cycle. A discharge capacity of 112 mAh g^{-1} is maintained at the 100th cycle.

It was recently reported that the cyclability of positive electrodes in sodium secondary batteries depends strongly on the solvents used [5]. For example, reduction products, such as sodium propyl carbonate, are reportedly generated on the sodium negative electrode surface by the reaction with PC that is the most commonly utilized solvent in sodium batteries. This species dissolves (although very slightly) into the electrolyte and can be oxidized on the positive electrode at top-of-charge, thereby limiting capacity utilization and causing low Coulombic efficiency. Even when carbon materials were utilized as a negative electrode in

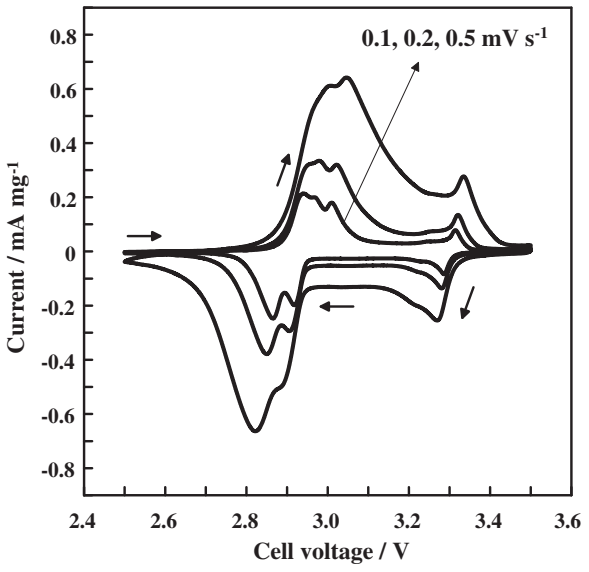

Fig. 2. Cyclic voltammograms of $NaCrO_2$ electrode in the NaFSA–KFSA ionic liquid acquired between 2.5 and 3.5 V at 363 K. Scan rates: 0.1, 0.2, and 0.5 mV s^{-1}.

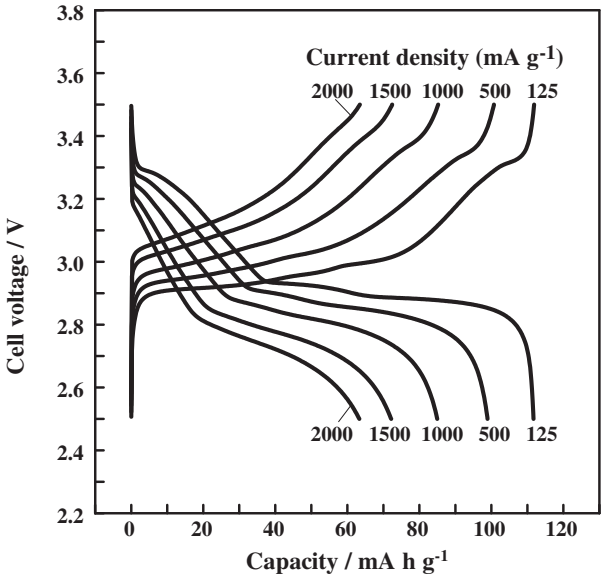

Fig. 3. Charge–discharge curves of $NaCrO_2$/NaFSA–KFSA/Na cell at 363 K. Charge–discharge rates: 125, 500, 1000, 1500, and 2000 mA g^{-1}. Cut-off voltage: 2.5–3.5 V.

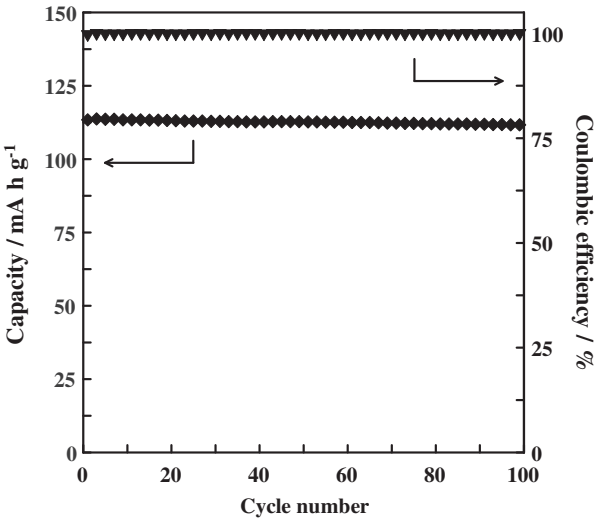

Fig. 4. Specific discharge capacity and Coulombic efficiency of $NaCrO_2$ positive electrode in NaFSA–KFSA ionic liquid as a function of cycle number at 363 K. Current density: 125 mA g^{-1}. Cut-off voltage: 2.5–3.5 V.

lieu of sodium metal, Na_2CO_3 and sodium alkyl carbonates were still found on the electrode surface as a major part of the SEI film [47,48]. Moreover, destructive oxidative decomposition of the electrolyte solution ($NaClO_4$/PC) and co-intercalation of solvent molecules are speculated to play a role in capacity fading [22]. Consequently, practical application requires either positive electrode surface treatments or the use of electrolyte additives such as fluoroethylene carbonate (FEC) [45,48]. In contrast to the carbonate-based electrolytes, the NaFSA–KFSA ionic liquid possesses good chemical and thermal stability, and it can be applied without the use of an additive.

The Na-driven structural transformation and the changes in the sodium composition at an intermediate temperature were evaluated using ex-situ XRD. Fig. 5 shows the XRD patterns of $Na_{1-x}CrO_2$ prepared at different states of charge. The $(003)_{hex}$ and $(104)_{hex}$ diffraction peaks (these peaks are indexed in the hexagonal setting), which belong only to the rhombohedral phase, are absent when $x > 0.2$. New diffraction peaks such as (001) for a monoclinic cell appear during further desodiation. Overall, the characteristic diffraction lines of the layered structure are observed at all compositions, indicating that the phase transitions occur as a consequence of slippage of the CrO_2 slabs without breaking of the Cr–O bonding. The composition-driven structural change is in the following sequence: rhombohedral O3 → monoclinic O′3 → monoclinic P′3. Schematic illustrations of the $Na_{1-x}CrO_2$ crystal structures are shown in Fig. 6. The lattice is made up of slabs of edge-sharing CrO_6 octahedra, between which Na^+ ions are inserted in an octahedral (O3) or trigonal prismatic (P3) environment. For each composition, the cationic distribution would thus result from the energy minimization between (1) the electrostatic repulsion that tends to separate the Na^+ ions in the *ab* plane, (2) the electron–electron interaction in the Cr layer, and (3) the Na^+–$Cr^{3+/4+}$ repulsion through the common face between the NaO_6 and CrO_6 polyhedra [39]. In order to facilitate comparison of the cell parameters, all samples were indexed in the monoclinic system. The hexagonal lattice parameters for the rhombohedral cell are related to the monoclinic cell parameters by the following relations [49]:

$$a_{hex} = a_{mon}/\sqrt{3}$$

$$b_{hex} = b_{mon}$$

$$c_{hex} = 3c_{mon}\sin\beta$$

The calculated Cr–Cr (in-plane distances, corresponding to the a_{mon} lattice parameter) and interslab distances (corresponding to c_{mon}) as a function of x in $Na_{1-x}CrO_2$ are plotted in Fig. 7. Notably, the interlayer *d*-spacing increases significantly when the Na ions are removed, as a result of the interruption of the balance of attractive forces between the Na ions and oxide anions and the repulsive forces between the oxide ions in the neighboring layers. The Cr–Cr intrasheet distance concomitantly declines as expected due to the oxidation of Cr^{3+} to the slightly smaller Cr^{4+} ions. These changes are in good agreement with those observed for most Na_xMO_2 layered oxides, implying that the sodium content is positively correlated to the structural cohesion [20,21,37,49].

There is a subtle difference between the sodium content at which phase transition begins in the present study compared to previous reports of room temperature evaluations. The onset of the phase transition seems to be more favorable at 363 K. In particular, the monoclinic P′3 structure of $Na_{1-x}CrO_2$ is detected at $x = 0.3$ in this study, whereas it is observed at $x = 0.4$ and 0.5 at room temperature [21]. It is not surprising that the desodiation kinetics is enhanced at the higher operating temperature used herein, and that the phase transitions are also facilitated. Given that Na ions in a prismatic coordination environment often exhibit higher ionic

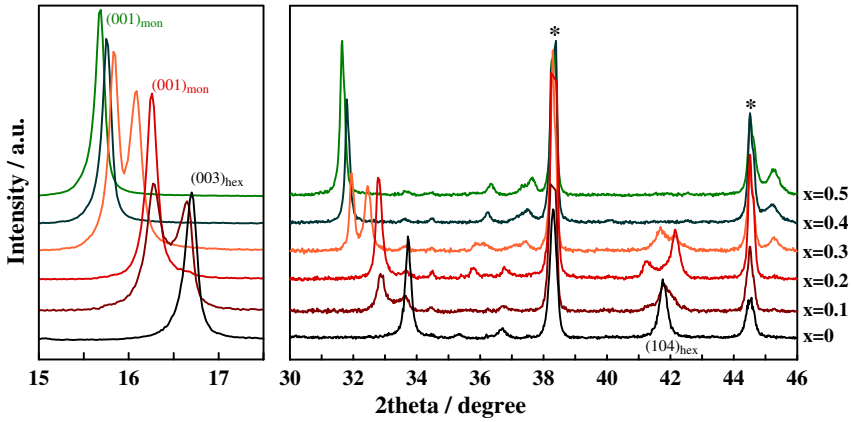

Fig. 5. XRD patterns of $Na_{1-x}CrO_2$ electrodes ($x = 0.1$, 0.2, 0.3, 0.4 and 0.5). The samples were electrochemically prepared in a $NaCrO_2$/NaFSA–KFSA/Na cell at 363 K. The XRD measurements were performed at room temperature. Peaks marked by an asterisk are assigned to the aluminum current collector. The $(003)_{hex}$ and $(104)_{hex}$ peaks are indexed in the hexagonal setting although the crystal system is rhombohedral.

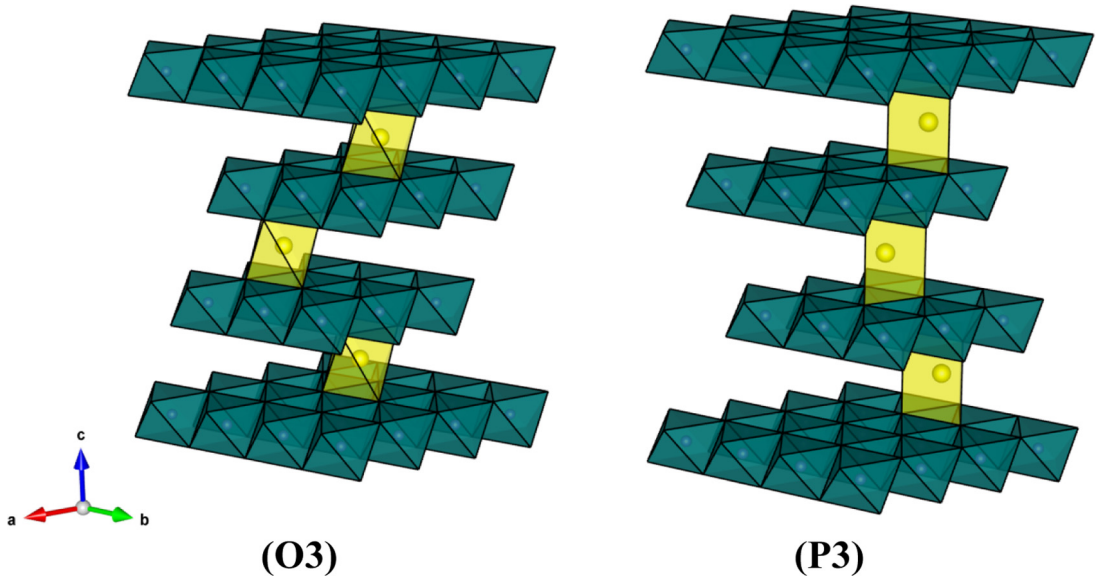

Fig. 6. Schematic illustrations of the crystal structure of $Na_{1-x}CrO_2$. Sodium ions are located at the octahedral and prismatic sites in the O3 and P3 types, respectively.

mobility than octahedrally coordinated congeners [41,50], a synergistic effect is clearly demonstrated by the enhanced rate capability obtained herein.

At present, Na-ion batteries are still in their early developmental stage. Major efforts have focused on studies at ambient temperature [1–6,16–22]. Whether these devices will perform as well at elevated temperatures as at ambient temperature remains a concern [51]. Although the ionic conductivity and reaction rate are expected to be enhanced at elevated temperatures, most organic solvent-based electrolytes are limited by the high volatility of the solvents utilized. Furthermore, the occurrence of unpredictable reactions between the electrolyte and electrode might negate the kinetic benefits [52]. Another justification for studies at elevated temperatures is that with high-pulse power operation, batteries become internally heated leading to rapid deterioration of their capacity and cycling property [51]. In such circumstances, the thermal stability of the NaFSA–KFSA ionic liquid is attractive for developing high-power and safe batteries.

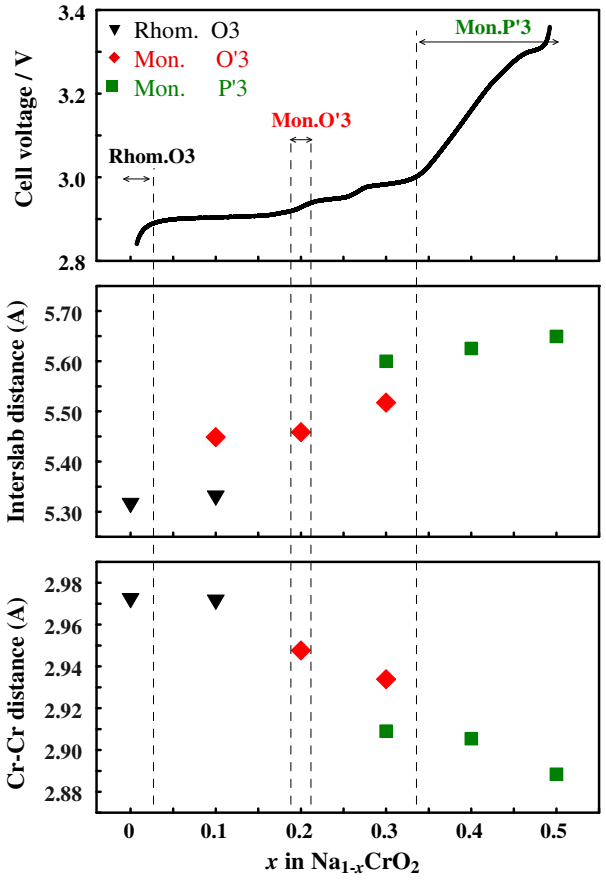

Fig. 7. Average Cr–Cr distances (bottom) and interslab distances (middle) of $Na_{1-x}CrO_2$ as a function of the x value, and the charge curve of the $NaCrO_2$/NaFSA–KFSA/Na cell measured at 5 mA g^{-1} at 363 K (top).

4. Conclusions

In summary, the charge–discharge behavior and phase transitions of the $NaCrO_2$ positive electrode were investigated in an intermediate temperature ionic liquid NaFSA–KFSA at 363 K. Electrochemical characterization revealed that the kinetics of the Na intercalation/deintercalation processes was enhanced and excellent cyclability was achieved versus when the same materials utilized in a conventional organic electrolyte at room temperature. The desodiation of $NaCrO_2$ resulted in the phase transition following the same sequence as in the case of room temperature charging: rhombohedral O3 → monoclinic O′3 → monoclinic P′3. The phase transitions were facilitated at high temperature relative to room temperature. The enhanced rate capability was attributed primarily to the facilitated Na intercalation/deintercalation kinetics.

Acknowledgments

This study was partly supported by Grants-in-Aid for Scientific Research A from the Japan Society for the Promotion of Science (JSPS) (No. 20246140) and the Advanced Low Carbon Technology Research and Development Program (ALCA) of the Japan Science and Technology Agency (JST).

References

[1] V. Palomares, P. Serras, I. Villaluenga, K.B. Hueso, J. Carretero-Gonzalez, T. Rojo, Energy Environ. Sci. 5 (2012) 5884–5901.

[2] S.P. Ong, V.L. Chevrier, G. Hautier, A. Jain, C. Moore, S. Kim, X.H. Ma, G. Ceder, Energy Environ. Sci. 4 (2011) 3680–3688.
[3] N. Yabuuchi, M. Kajiyama, J. Iwatate, H. Nishikawa, S. Hitomi, R. Okuyama, R. Usui, Y. Yamada, S. Komaba, Nat. Mater. 11 (2012) 512–517.
[4] J. Barker, M.Y. Saidi, J.L. Swoyer, Electrochem. Solid-State Lett. 6 (2003) A1–A4.
[5] C. Vidal-Abarca, P. Lavela, J.L. Tirado, A.V. Chadwick, M. Alfredsson, E. Kelder, J. Power Sources 197 (2012) 314–318.
[6] N. Yabuuchi, H. Yoshida, S. Komaba, Electrochemistry 80 (2012) 716–719.
[7] P. Barpanda, J.N. Chotard, N. Recham, C. Delacourt, M. Ati, L. Dupont, M. Armand, J.M. Tarascon, Inorg. Chem. 49 (2010) 7401–7413.
[8] V.L. Chevrier, G. Ceder, J. Electrochem. Soc. 158 (2011) A1011–A1014.
[9] J.F. Whitacre, A. Tevar, S. Sharma, Electrochem. Commun. 12 (2010) 463–466.
[10] S.W. Kim, D.H. Seo, X.H. Ma, G. Ceder, K. Kang, Adv. Energy Mater. 2 (2012) 710–721.
[11] J.L. Sudworth, J. Power Sources 11 (1984) 143–154.
[12] J. Coetzer, J. Power Sources 18 (1986) 377–380.
[13] C.H. Dustmann, J. Power Sources 127 (2004) 85–92.
[14] X.C. Lu, G.G. Xia, J.P. Lemmon, Z.G. Yang, J. Power Sources 195 (2010) 2431–2442.
[15] S.F. Song, Z.Y. Wen, Y. Liu, J. Lin, X.G. Xu, Q.X. Zhang, J. Solid State Electrochem. 14 (2010) 1735–1740.
[16] B.L. Ellis, W.R.M. Makahnouk, Y. Makimura, K. Toghill, L.F. Nazar, Nat. Mater. 6 (2007) 749–753.
[17] I.D. Gocheva, M. Nishijima, T. Doi, S. Okada, J. Yamaki, T. Nishida, J. Power Sources 187 (2009) 247–252.
[18] Y. Yamada, T. Doi, I. Tanaka, S. Okada, J. Yamaki, J. Power Sources 196 (2011) 4837–4841.
[19] N. Recham, J.N. Chotard, L. Dupont, K. Djellab, M. Armand, J.M. Tarascon, J. Electrochem. Soc. 156 (2009) A993–A999.
[20] S. Komaba, N. Yabuuchi, T. Nakayama, A. Ogata, T. Ishikawa, I. Nakai, Inorg. Chem. 51 (2012) 6211–6220.
[21] S. Komaba, T. Nakayama, A. Ogata, T. Shimizu, C. Takei, S. Takada, A. Hokura, I. Nakai, ECS Trans. 16 (2009) 43–55.
[22] S. Komaba, C. Takei, T. Nakayama, A. Ogata, N. Yabuuchi, Electrochem. Commun. 12 (2010) 355–358.
[23] K. Xu, Chem. Rev. 104 (2004) 4303–4417.
[24] R.S. Kuhnel, N. Bockenfeld, S. Passerini, M. Winter, A. Balducci, Electrochim. Acta. 56 (2011) 4092–4099.
[25] M. Armand, F. Endres, D.R. MacFarlane, H. Ohno, B. Scrosati, Nat. Mater. 8 (2009) 621–629.
[26] B. Scrosati, J. Garche, J. Power Sources 195 (2010) 2419–2430.
[27] S.K. Martha, E. Markevich, V. Burgel, G. Salitra, Z. Zinigrad, B. Markovsky, H. Sclar, Z. Pramovich, O. Heik, D. Aurbach, I. Exnar, H. Buqa, T. Drezen, G. Semrau, M. Schmidt, D. Kovacheva, N. Saliyski, J. Power Sources 189 (2009) 288–296.
[28] M. Egashira, T. Tanaka, N. Yoshimoto, M. Morita, Electrochemistry 80 (2012) 755–758.
[29] R. Hagiwara, K. Tamaki, K. Kubota, T. Goto, T. Nohira, J. Chem. Eng. Data 53 (2008) 355–358.
[30] K. Kubota, K. Tamaki, T. Nohira, T. Goto, R. Hagiwara, Electrochim. Acta 55 (2010) 1113–1119.
[31] K. Kubota, T. Nohira, T. Goto, R. Hagiwara, Electrochem. Commun. 10 (2008) 1886–1888.
[32] K. Kubota, T. Nohira, R. Hagiwara, J. Chem. Eng. Data 55 (2010) 3142–3146.
[33] A. Watarai, K. Kubota, M. Yamagata, T. Goto, T. Nohira, R. Hagiwara, K. Ui, N. Kumagai, J. Power Sources 183 (2008) 724–729.
[34] T. Nohira, T. Ishibashi, R. Hagiwara, J. Power Sources 205 (2012) 506–509.
[35] A. Fukunaga, T. Nohira, Y. Kozawa, R. Hagiwara, S. Sakai, K. Nitta, S. Inazawa, J. Power Sources 209 (2012) 52–56.
[36] T. Yamamoto, T. Nohira, R. Hagiwara, A. Fukunaga, S. Sakai, K. Nitta, S. Inazawa, J. Power Sources 217 (2012) 479–484.
[37] M. Sathiya, K. Hemalatha, K. Ramesha, J.M. Tarascon, A.S. Prakash, Chem. Mater. 24 (2012) 1846–1853.
[38] C. Delmas, C. Fouassier, P. Hagenmuller, Physica B & C 99 (1980) 81–85.
[39] R. Berthelot, D. Carlier, C. Delmas, Nat. Mater. 10 (2011) 74–80.
[40] M. Blangero, D. Carlier, M. Pollet, J. Darriet, C. Delmas, J.P. Doumerc, Phys. Rev. B 77 (2008) 184116-1–184116-8.
[41] C. Delmas, J.J. Braconnier, C. Foussier, P. Hagenmuller, Solid State Ionics 3–4 (1981) 165–169.
[42] Z.H. Lu, J.R. Dahn, J. Electrochem. Soc. 148 (2001) A1225–A1229.
[43] M. D'Arienzo, R. Ruffo, R. Scotti, F. Morazzoni, C.M. Maria, S. Polizzi, Phys. Chem. Chem. Phys. 14 (2012) 5945–5952.
[44] X.H. Rui, N. Ding, J. Liu, C. Li, C.H. Chen, Electrochim. Acta 55 (2010) 2384–2390.
[45] J.J. Ding, Y.N. Zhou, Q. Sun, Z.W. Fu, Electrochem. Commun. 22 (2012) 85–88.
[46] S. Seki, Y. Kobayashi, H. Miyashiro, Y. Ohno, A. Usami, Y. Mita, N. Kihira, M. Watanabe, N. Terada, J. Phys. Chem. B 21 (2006) 10229–10230.
[47] M.D. Slater, D. Kim, E. Lee, C.S. Johnson, Adv. Funct. Mater. 23 (2013) 947–958.
[48] S. Komaba, T. Ishikawa, N. Yabuuchi, W. Murata, A. Ito, Y. Ohsawa, ACS Appl. Mater. Interfaces 3 (2011) 4165–4168.
[49] I. Saadoune, A. Maazaz, M. Menetrier, C. Delmas, J. Solid State Chem. 122 (1996) 111–117.
[50] C. Delmas, A. Maazaz, C. Fouassier, J.M. Reau, P. Hagenmuller, Mater. Res. Bull. 14 (1979) 329–335.
[51] H. Deng, I. Belharouak, C.S. Yoon, Y.K. Sun, K. Amine, J. Electrochem. Soc. 157 (2010) A1035–A1039.
[52] D.H. Jang, Y.J. Shin, S.M. Oh, J. Electrochem. Soc. 143 (1996) 2204–2211.